

Radiation reaction induced harmonics generation in ultra-relativistic intense laser interaction with plasmas

J Y Yu^{1,2} , M Chen^{1,2,4} , W Y Liu^{1,2} , S M Weng^{1,2}  and Z M Sheng^{1,2,3,4} 

¹Key Laboratory for Laser Plasmas (MOE), School of Physics and Astronomy, Shanghai Jiao Tong University, Shanghai, 200240, People's Republic of China

²Collaborative Innovation Center of IFSA (CICIFSA), Shanghai Jiao Tong University, Shanghai 200240, People's Republic of China

³SUPA, Department of Physics, University of Strathclyde, Glasgow G4 0NG, United Kingdom

E-mail: minchen@sjtu.edu.cn and zsheng@sjtu.edu.cn

Received 13 December 2019, revised 24 February 2020

Accepted for publication 27 February 2020

Published 16 March 2020



Abstract

A new mechanism of harmonics generation is found in ultraintense laser interactions with plasmas, where radiation reaction effects dominate. The radiation reaction results in trapped electrons which oscillate in the laser field and emit high energy photons. Such emission event happens with a frequency spectrum containing double or high order components of the drive laser, inducing second and higher order harmonics emission. Although the intensity of such harmonics is too weak for practical applications, they could be used as a specific diagnostic to detect the radiation reaction effects in the upcoming experimental studies of the extremely intense laser pulse interacting with plasmas.

Keywords: laser plasma interaction, radiation reaction, harmonics generation

(Some figures may appear in colour only in the online journal)

1. Introduction

Attosecond extreme ultraviolet (XUV) pulses are widely used in detecting ultrafast dynamics of atoms, molecular and condensed matter [1, 2]. Laser-plasma induced high-order harmonics generation (HHG) is an effective way to produce such XUV sources. The first HHG experiment was reported in 1987 by McPherson *et al*, using a picosecond pulse interacting with rare gases [3]. The involved mechanism is due to the nonlinear motion of bounded electrons in the laser fields at relatively low intensity. Harmonics can also be generated by a low intensity q-Gaussian laser beam propagating in a preformed parabolic plasma channel [4–6], where the generated density gradients excite an electron plasma wave at pump frequency that interacts with the pump beam to produce harmonics. With the help of advanced laser technologies, laser power now can be delivered into hundreds terawatt or even pettawatt scale [7]. With such high laser intensity, the

harmonics generation mainly comes from laser solid interaction, where the electrons oscillate and radiate around the target surface, or excite a wakefield along the density upramp in the front part of a solid target which then transforms to electromagnetic wave through mode conversion. Ultrathin electron sheet can also be generated and coherently radiate high harmonics. Such processes are explained by relativistic oscillating mirror (OM), coherent wake emission (CWE) and coherent synchrotron emissions (CSE) [8–11]. Due to the high resolution and high brilliance of laser solid harmonics, they are used in ultrafast physics and laser plasma diagnostics [12, 13].

At even higher laser power when the focused laser intensity is higher than 10^{20} W cm⁻², the radiation reaction (RR) effects may not be neglected especially for the two-counter propagating laser pulse interacting with a solid target. The radiation reaction is usually regarded as the recoil force on the electron when a high energy photon is emitted. RR effects can induce beam cooling, longitudinal magnetic field formation and electron trapping [14–16], but it is also quite

⁴ Authors to whom any correspondence should be addressed.

important for high energy photon emission. In this laser intensity regime, by using special target structure such as micro-wire target, ultra-bright attosecond gamma-ray generation were proposed and numerically demonstrated by different groups [17, 18]. In laser interaction with near critical density plasmas, a new gamma-ray emission mechanism named transversely oscillating electron synchrotron emission has also been proposed [19]. These studies show the great potential of using high power laser to generate high frequency emission. In experiments, recently, two groups have detected RR effects in laser plasma interaction with laser intensity $\sim 10^{20} \text{ W cm}^{-2}$ [20, 21]. However, clear and convenient detection of RR and especially its effects on harmonics generation are still required.

When the laser intensity continues increasing, laser plasma interaction reaches a strong relativistic, or quantum electrodynamics (QED) dominated regime. Some related works concerning harmonics generation from such intense laser interaction with solid surface plasmas have been reported. Liu *et al* reported a method to generate gamma-ray train, which is strongly related to the stochasticity of the radiation in QED regime [22]. Tang *et al* studied the frequency shift and spectrum broadening of the generated harmonics and proposed an optimum configuration for short-wavelength radiation [23]. By using classical or semi-classical theory, Li *et al* have investigated high harmonics generation from free electrons interacting with intense laser fields, where the Landau–Lifshitz equation is used to describe the radiation reaction. The frequency shift and the angular power distribution were studied in detail [24]. In the electron-laser head-on Thomson scattering configuration, Ruijter *et al* have proposed an analytical explanation for the harmonic spectral broadening due to RR effects [25]. For even higher laser intensity, Yu *et al* have shown that QED cascade effects can introduce harmonics generation when a two-counter propagating laser target interaction configuration is used. The harmonics can be used as a tool to detect the QED-cascade processes [26].

In this paper, by using Particle-In-Cell (PIC) simulations, we show a new mechanism of harmonics generation related to RR effects, which can be used as a diagnostic for RR effects in the coming extreme intense laser plasma interaction. As we show in this condition the normal mechanism for harmonics generation, such as OM, CWE, CSE are absent. When an ultra-relativistic intense laser beam propagates through plasma, some electrons are transversely trapped inside the laser pulse due to RR effects [27]. The trapped electrons then emit high energy photons with an emission frequency related to the laser frequency and its harmonics, which induces the harmonics emission. Such harmonics generation and propagation depend on the target thickness. For a thin target, the laser will penetrate through the target and breaks the harmonics generation. For a thick target, the laser will be strongly absorbed and the hole boring depth is largely reduced due to RR effect, as a result, the forward transmitting harmonics get much weak. Only with an optimal plasma thickness, when both the generation and transmission processes are well treated, RR effects induced forward harmonics emission can be observed.

2. Simulation setup

In our studies the fully relativistic PIC code EPOCH with radiation reaction module has been used to conduct the two-dimensional (2D) simulations [28, 29]. A linearly polarized laser pulse with wavelength of $\lambda_0 = 1 \mu\text{m}$, and normalized peak intensity of $a_0 = 500$ propagates along x direction. Here $a_0 = eE_L/m_e\omega_0c$, e and m_e are the electron charge and mass, respectively. ω_0 is the laser frequency and c is the speed of light in vacuum. The laser pulse has both Gaussian profiles in longitudinal and transverse directions with duration of $\tau = 20T_0$ and spot radius of $r_0 = 5\lambda_0$. The simulation box is $80\lambda_0 \times 40\lambda_0$ large in $x \times y$ directions with a cell size of $0.01\lambda_0 \times 0.05\lambda_0$. The target is initially composed of electrons and protons with initial electron density $n_e = 20n_c$, where $n_c = m_e\omega_0^2/4\pi e^2$ is the critical density for the drive laser. The left boundary of the target is at $x = 10\lambda_0$ and in the simulations we scan the thickness of the target to study its effects on harmonics generation. With our simulation parameters, RR effects are not negligible. However, the electron-positron pair production and the QED cascade process have no observable effects on the final results and both of them are neglected. Additional test simulations have been performed to confirm the rationality of the neglect. In fact, for single laser interacting with plasma, considerable pair production requires laser with much higher intensity, or high Z targets via the Bethe–Heitler process [30–33].

3. Simulation results and harmonics generation

Before studying the RR effects induced harmonic generation, we firstly investigate the laser absorption process. Typical simulation results of plasma density distribution, laser evolution and energy absorption are shown in figure 1. Two simulations with identical laser plasma parameters but with or without RR module are performed. Electron density and laser field distributions at $t = 40 T_0$ for target with initial thickness of $50\lambda_0$ are shown in figures 1(a) and (c) for the case with RR and in figures 1(b) and (d) for the case without RR. For both cases, the electrons are expelled both longitudinally and transversely by the strong laser ponderomotive force and a plasma cavity is generated, with dense electron layers formed around the boundary of the cavity. Meanwhile, in the case with RR, some electrons are trapped and quivering in the laser fields, they finally gather near the $y = 0$ axis. Such trapping effect has been firstly studied by Ji *et al* and the phenomenon is absent when the RR module is switched off [27]. Besides the trapped electrons, in the RR case, the laser front side shows more unstable characters, the drive laser has been split into three filaments. Although the laser bifurcation also happens during normal laser plasma interaction, in the current two cases, such bifurcation happens earlier in the RR case [34, 35]. The transverse size of the tip of the plasma cavity is also larger in the RR case.

Along with the strong quivering of trapped electrons inside the intense laser, the emitted photons from these

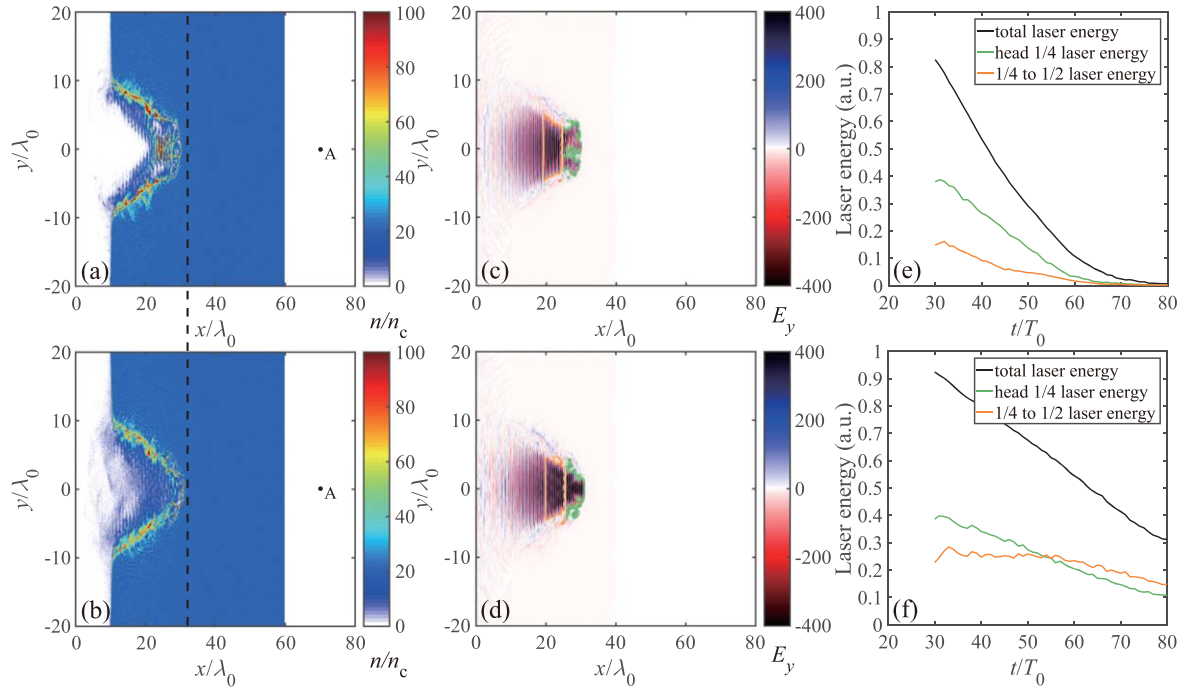


Figure 1. Spatial electron density distributions at $t = 40 T_0$ for the cases with RR (a) and without RR (b), respectively. A is the detection point used below. Laser field distributions at $t = 40 T_0$ for the cases with RR (c) and without RR (d). The temporal evolution of the total and different part of the laser energy for the cases with RR (e) and without RR (f).

electrons have both forward and sideward momenta, giving the RR force both in backward and inward directions, so the electrons are trapped in the middle area of the laser pulse and comove with it. Such plasma distribution makes the laser absorption more efficient. Unlike the usual pulse front dominated absorption, i.e. laser absorption by pulse front etching, in the RR case, the effective absorption region of the laser pulse is enlarged. To clearly show such process, according to the instant laser profile, we trace the laser energy evolution for two different parts: the front 1/4 part and the following 1/4 to 1/2 part as labelled by the vertical orange lines in figures 1(c) and (d). In figures 1(e) and (f), we show the temporal evolution of the laser energies around these two parts. The black line represents the evolution of the total laser energy in the simulation box. The green and orange lines represent the evolution of the first and second quarter parts of the laser energy, respectively. As one can see, for the RR case, the laser field energy drops exponentially, which is much faster than the linear decrease in the case without RR. The energies both in the two labeled parts are decreased simultaneously. However, in the case without RR effect, the laser energy in the second quarter part almost does not change for the initial stage which means there is no laser absorption there. This is easily understood from the electron density distribution. The trapped electrons in the RR case just stay in the second quarter part of the laser. The laser energy there is absorbed by the trapped electrons. Since the laser intensity is high enough, high energy photons emitted by these trapped electrons have reaction effects on the electrons, which alters

the electrons' trajectories. In some cases, when this kind of alteration has some periodical component, it can induce harmonic currents in the plasma and excite harmonic radiations. In the following we focus on such process to see how the low frequency harmonic radiation is generated and propagates.

To clearly show the harmonics generation and propagation in the forward direction, we have chosen a detection point A, whose coordinate is $(70,0)$ behind the target as marked in figures 1(a) and (b). Figure 2(a) shows the Fourier spectra of the right-propagating fields go through the detection point A for the simulations with RR (magenta line) and without RR (gray line). Here the initial target thickness is $30\lambda_0$. The right-propagating field is defined as $F_r = (E_y + B_z)/2$, where E_y is the electric field and B_z the magnetic field. It is clear that both cases appear 2nd and 3rd harmonic components. For such thin target, the intensity of HG in the RR case is stronger than that in the case without RR. To make the comparison much clearer, the intensities for the case with RR and without RR are illustrated in figure 2(b). For the case without RR (dashed lines), the intensity of both 2nd and 3rd harmonic components do not change much with the target thickness. When the target is thin, the intensities of harmonics components of the RR case are larger than the case without RR. However, when the target becomes thicker, the harmonics intensities of the RR case outside of the plasma drop quickly due to the smaller laser hole boring depth and the following larger HG penetration distance inside the plasma. When the target thickness is $50\lambda_0$, harmonics intensities for the RR case almost disappear.

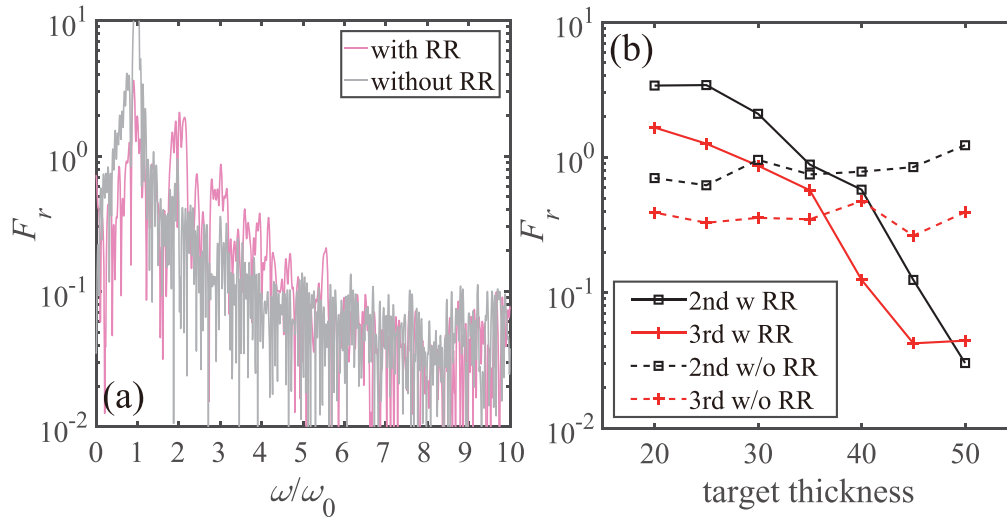


Figure 2. (a) Fourier transform of the right-propagating field component at detection point A for the cases with RR (magenta line) and without RR (gray lines). The target thickness used here is $30\lambda_0$. (b) The intensity of 2nd (black lines) and 3rd (red lines) harmonic components for the cases with (solid lines) and without (dashed lines) RR.

4. Radiation reaction effects on harmonics generation

From the above simulation results, we can see that in the RR case the HG is enhanced, which means besides the usual mechanism for second and third harmonic generation, the RR effect may induce a new kind of harmonic generation, which is still not clear yet. To investigate this kind of new mechanism, we plot the electric current density and trace some trapped electrons' trajectories. Figures 3(a) and (b) are the spatial distribution of the electric current density at $t = 40 T_0$ for the cases with RR and without RR, respectively. The black line denotes the boundary of the laser fields at that moment. The electric current density is enormous at the field boundary and the area with trapped electrons. Both of them correspond to a massive electron density, which is understandable since the current density highly relies on the charge density. The difference of the two cases mainly comes from the area where the electrons are trapped.

We focus on the trapped electrons' motion for the RR case in figures 3(c) and (d). Figures 3(c)-i and (d)-i show the trajectories of the selected trapped electrons. From the trajectories, one can see that the electrons are firstly expelled by the laser ponderomotive force, then they oscillate in the transverse direction and move forwards. These electrons are trapped due to the radiation recoil force as explained by Ji *et al* [27]. Whenever an electron emits a photon, it loses energy and momentum, and this results in a sudden change of the local current density. In the code we have added a new variable named high energy photon emission event (HEPEE) to the particle tracking module. Whenever a high energy photon is emitted, the HEPEE variable of the electron increases. When we track these selected electrons' positions and momenta, we also record the HEPEE for every selected electron at every simulation step. Due to the limitation of numerical simulation, we can only record one event in each simulation step, thus a binary-code like emission spectrum is

recorded by the modified code. To further analyze the photon emission, this binary-code like emission spectrum has been re-organized by merging the emission number during 6 neighbouring steps to a single counting step, which means that the maximum value of HEPEE for a single electron at a counting step is 6. In addition, each photon emission time has been transformed to the retarded time relative to the detection point, which corresponds to the time when the emitted electromagnetic wave has arrived the detection point. It is defined as $t_A = t_e + |\mathbf{r}_A - \mathbf{r}_e|/c$, where t_e is the emission time of the high energy photon in the laboratory frame, \mathbf{r}_A and \mathbf{r}_e are the coordinates of the detection point and the local emission point. The temporal evolution of HEPEE with retarded time of the two chosen electrons are shown in figures 3(c)-ii and (d)-ii. The bar-code like figure also indicates the stochastic nature of the high energy photon emission. The Fourier transform of the HEPEEs of the two selected electrons is given in figures 3(c)-iii and (d)-iii. As it is shown clearly that there are 2nd and 3rd frequency components of photon emission in these figures. Such frequency corresponds to a double or triple emission in one laser period, where the double frequency majors. The double frequency can be understood since the high energy photon emission usually happens at the electric peaks of the laser pulse.

For each electron in the trapping area, RR results in the HEPEE with double or high order frequency component. To see the coherence of each electron's HEPEE, we show the temporal evolution of the radiated energy from all of the trapped electrons with respect to the retarded time of point A in figure 4(a). As one can see that the envelope of the radiation energy evolution acts exactly like the incident laser envelope and there are periodic peaks on this envelope line, which means the HEPEEs of the trapped electrons are somewhat coherent. The corresponding Fourier transform is shown in figure 4(b), where the fundamental frequency dominates the spectrum, with also 2nd and 3rd components of a moderate low intensity. Such spectrum can be regarded as a

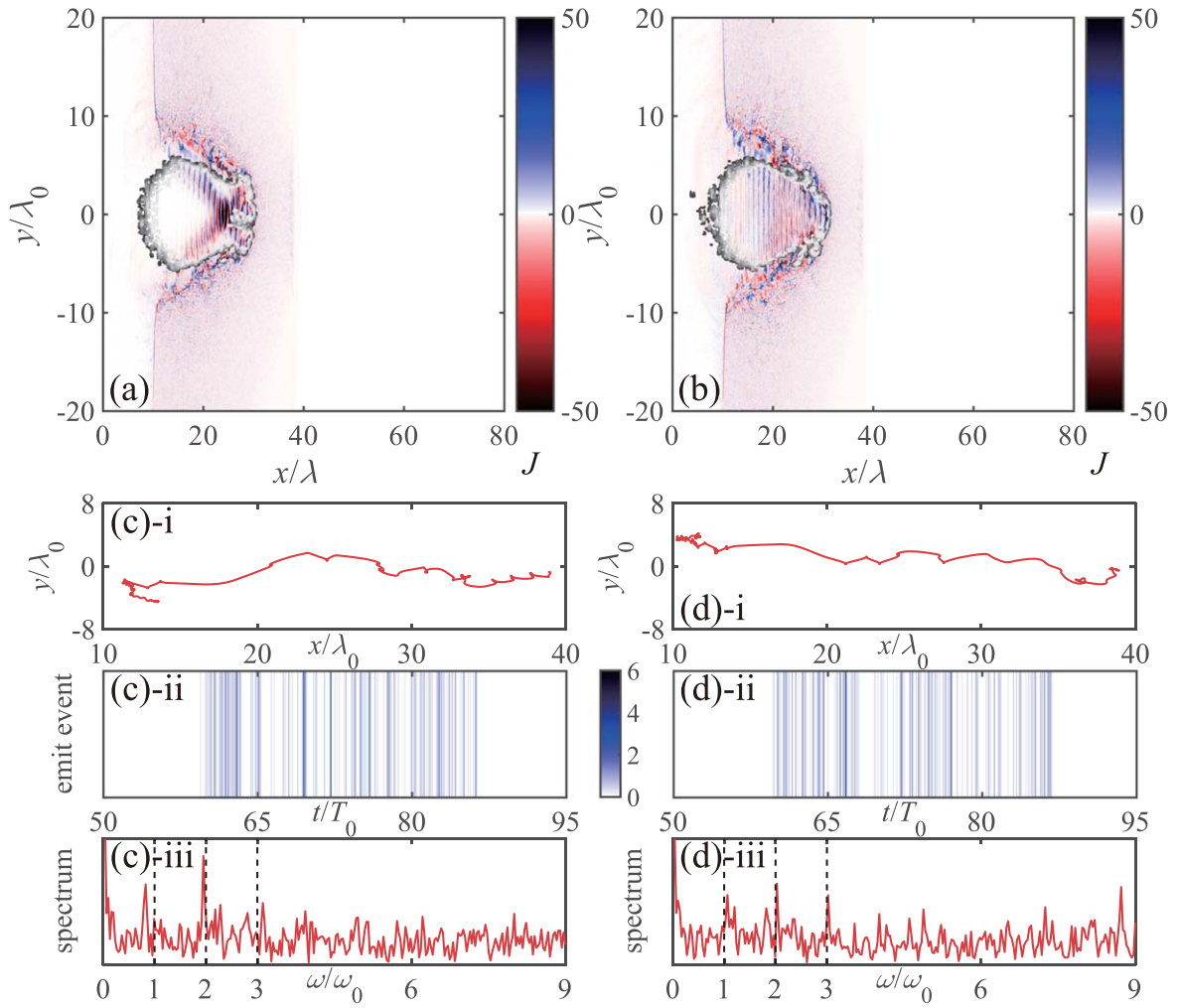


Figure 3. Spatial distributions of electric current density at $t = 40T_0$ for the cases with RR (a) and without RR (b). The black line denotes the boundary of the laser field area. (c) And (d) are typical trajectories (i), high energy photon emission events (ii) and the corresponding FFT of the emission event (iii) for the two selected electrons in the simulation case with RR.

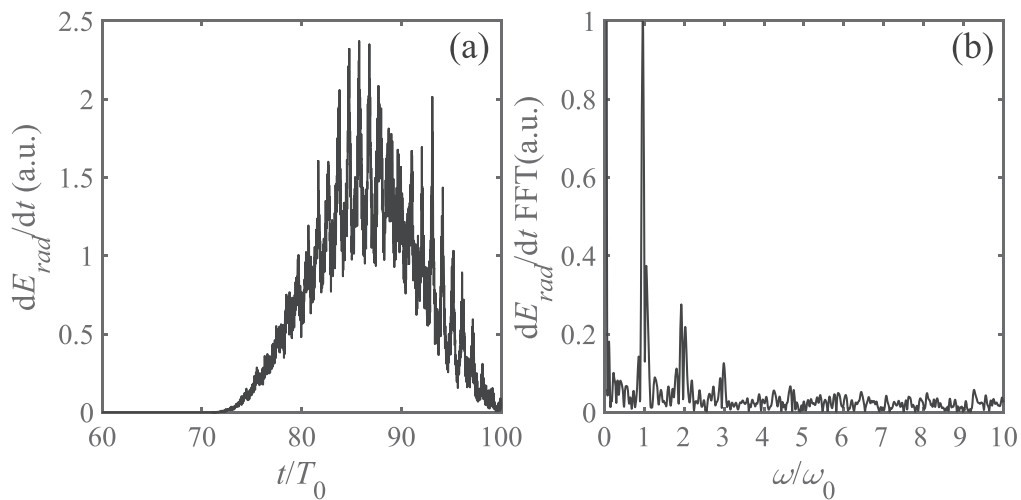


Figure 4. The temporal evolution of the radiated energy from all of the trapped electrons (a) and its corresponding FFT (b). Here the horizontal coordinate has been transformed to the retarded time for the detection point for the subfigure (a).

coherent superposition of HEPEEs of each trapped electron. This is understandable since most of such emissions are locked to the same laser phase (i.e. emission mainly happens at the peaks of the electric field), the alterations of these electrons' motion can then be somewhat phase locked. The collective alteration of the electrons' momenta results in a local electric current. The current inherits the frequency components of the HEPEE, and thus the harmonic radiation can be induced.

To show the radiation coherence in an easily understood way, we compare the current mechanism with the normal HHG from laser gas interaction with moderate intensity [36], where usually a three-step model is used to explain the harmonics generation process [37]. In our case, i.e. laser solid interaction with RR, high energy photon emission from the free electrons takes similar role as the electron ionization from the gas atoms in the normal laser gas interaction. Both of them trigger the local current alteration. The difference is that in our case, the harmonics generation is not due to the ionized electrons accelerating in the drive laser field, but due to the radiation reaction effects of the 'ionized' high energy photon on its mother electron. The radiation reaction excites the local current variation. The phase matching of radiation from different electrons are satisfied due to the high energy photon emission locked to the drive laser's peak electric field, which is similar as the atomic ionization process locked to the peak field of the laser. However, such HEPEE has stochastic character and the 'ionized electrons' only occupy a small amount of the whole electrons, the coherency of the harmonics generation is not as high as the normal gas HHG process, thus high order harmonics are largely suppressed and only low order harmonics are prominent.

In our studies it is found when RR effects are included, both the 2nd and 3rd frequency components of the radiation energy evolution can be seen in all of the simulations with different target thickness, even though the intensities of the harmonics radiation are different. This is because of the harmonics propagation effect. In the thick target case with RR, the harmonics will be absorbed by the target and at the same time the laser energy is also quickly and intensely absorbed, hence RR induced HG gets much smaller when the target thickness increases. In the case without RR, the laser can finally penetrate the target and the harmonics can easily transmit through the target and its intensity is weakly dependent on the target thickness as shown in figure 2(b).

5. Conclusion and summary

To conclude, a new mechanism of harmonic generation due to the RR effect is found. When an intense laser beam irradiates a relativistically underdense plasma, some electrons are trapped in the laser located region. These electrons emit photons and give them transverse momenta. Such photon emission is locked to the laser pulse, which makes all the electrons' emissions are coherently related and the emission rate shows 2nd and higher order frequency components of the fundamental laser frequency. The RR thus induces an electric

current inside the plasma, which finally induced the harmonics generation. Due to the strong absorption of laser energy, such HG drops quickly when the target thickness increases. Such thickness dependent harmonics emission gives a possible way to detect the RR effects in the near future pettawatt laser plasma interactions.

Acknowledgments

The work was supported by National Natural Science Foundation of China (Grant Nos. 11721091 and 11774227) and Science Challenge Project (TZ2018005). Simulations were performed on the II Supercomputer at Shanghai Jiao Tong University and Tianhe II supercomputer at Guangzhou.

ORCID iDs

J Y Yu  <https://orcid.org/0000-0002-8753-7235>

M Chen  <https://orcid.org/0000-0002-4290-9330>

W Y Liu  <https://orcid.org/0000-0001-6659-8250>

S M Weng  <https://orcid.org/0000-0001-7746-9462>

Z M Sheng  <https://orcid.org/0000-0002-8823-9993>

References

- [1] Krausz F and Ivanov M 2009 *Rev. Mod. Phys.* **81** 163–234
- [2] Tao Z, Chen C, Szilvási T, Keller M, Mavrikakis M, Kapteyn H and Murnane M 2016 *Science* **353** 62–7
- [3] McPherson A, Gibson G, Jara H, Johann U, Luk T S, McIntyre I A, Boyer K and Rhodes C K 1987 *J. Opt. Soc. Am. B* **4** 595–601
- [4] Gupta N 2019 *Laser Part. Beams* **37** 184–96
- [5] Singh A and Gupta N 2014 *Laser Part. Beams* **32** 621–9
- [6] Gupta N, Singh N and Singh A 2015 *Phys. Plasmas* **22** 113106
- [7] Mourou G A, Fisch N J, Malkin V M, Toroker Z, Khazanov E A, Sergeev A M, Tajima T and Le Garrec B 2012 *Opt. Commun.* **285** 720–4
- [8] Baeva T, Gordienko S and Pukhov A 2006 *Phys. Rev. E* **74** 046404
- [9] Quéré F, Thauray C, Monot P, Dobosz S, Martin P, Geindre J P and Audebert P 2006 *Phys. Rev. Lett.* **96** 125004
- [10] Dromey B *et al* 2012 *Nat. Phys.* **8** 804–8
- [11] Gonoskov A A, Korzhimanov A V, Kim A V, Marklund M and Sergeev A M 2011 *Phys. Rev. E* **84** 046403
- [12] Teubner U, Eidmann K, Wagner U, Andiel U, Pisani F, Tsakiris G D, Witte K, Meyer-ter-Vehn J, Schlegel T and Förster E 2004 *Phys. Rev. Lett.* **92** 185001
- [13] Leblanc A, Denoëud A, Chopineau L, Menerat G, Martin P and Quéré F 2017 *Nat. Phys.* **13** 440–3
- [14] Yoffe S R, Kravets Y, Noble A and Jaroszynski D A 2015 *New J. Phys.* **17** 053025
- [15] Liseykina T V, Popruzhenko S V and Macchi A 2016 *New J. Phys.* **18** 072001
- [16] Gonoskov A, Bashinov A, Gonoskov I, Harvey C, Ilderton A, Kim A, Marklund M, Mourou G and Sergeev A 2014 *Phys. Rev. Lett.* **113** 014801
- [17] Léczy Z and Andreev A 2019 *Phys. Rev. E* **99** 013202
- [18] Li H Z, Yu T P, Hu L X, Yin Y, Zou D B, Liu J X, Wang W Q, Hu S and Shao F Q 2017 *Opt. Express* **25** 21583

- [19] Chang H X, Qiao B, Zhang Y X, Xu Z, Yao W P, Zhou C T and He X T 2017 *Phys. Plasmas* **24** 043111
- [20] Cole J M *et al* 2018 *Phys. Rev. X* **8** 011020
- [21] Poder K *et al* 2018 *Phys. Rev. X* **8** 031004
- [22] Liu C, Shen B F, Zhang X M, Ji L L, Wang W P, Xu J C, Zhao X Y, Yi L Q, Shi Y, Zhang L G *et al* 2016 *Phys. Plasmas* **23** 083120
- [23] Tang S, Kumar N and Keitel C H 2017 *Phys. Rev. E* **95** 051201
- [24] Li A K, Wang J X, Ren N, Zhu W J, Li X Y, Hoehn R and Kais S 2014 *Laser Phys.* **24** 015302
- [25] Ruijter M, Kharin V Y and Rykovanov S G 2018 *J. Phys. B: At. Mol. Opt. Phys.* **51** 225701
- [26] Yu J Y, Yuan T, Liu W Y, Chen M, Luo W, Weng S M and Sheng Z M 2018 *Plasma Phys. Control. Fusion* **60** 044011
- [27] Ji L L, Pukhov A, Kostyukov I Y, Shen B F and Akli K 2014 *Phys. Rev. Lett.* **112** 145003
- [28] Arber T D *et al* 2015 *Plasma Phys. Control. Fusion* **57** 113001
- [29] Ridgers C P, Kirk J G, Duclous R, Blackburn T G, Brady C S, Bennett K, Arber T D and Bell A R 2014 *J. Comput. Phys.* **260** 273–85
- [30] Yuan T, Chen M, Yu J Y, Liu W Y, Luo W, Weng S M and Sheng Z M 2017 *Phys. Plasmas* **24** 063104
- [31] Ridgers C P, Brady C S, Duclous R, Kirk J G, Bennett K, Arber T D, Robinson A P L and Bell A R 2012 *Phys. Rev. Lett.* **108** 165006
- [32] Sarri G *et al* 2013 *Phys. Rev. Lett.* **110** 255002
- [33] Chen H, Wilks S C, Bonlie J D, Liang E P, Myatt J, Price D F, Meyerhofer D D and Beiersdorfer P 2009 *Phys. Rev. Lett.* **102** 105001
- [34] Li G, Yan R, Ren C, Tonge J and Mori W B 2011 *Phys. Plasmas* **18** 042703
- [35] Li G, Yan R, Ren C, Wang T L, Tonge J and Mori W B 2008 *Phys. Rev. Lett.* **100** 125002
- [36] Kapteyn H C, Murnane M M and Christov I P 2005 *Phys. Today* **58** 39–46
- [37] Corkum P B 1993 *Phys. Rev. Lett.* **71** 1994–7